© 2016. Published by The Company of Biologists Ltd | Journal of Cell Science (2016) 129, 502-516 doi:10.1242/jcs.179333

RESEARCH ARTICLE

Emery–Dreifuss muscular dystrophy mutations impair TRC40-mediated targeting of emerin to the inner nuclear membrane

Janine Pfaff[1,*], Jhon Rivera Monroy[1,*], Cara Jamieson[1], Kalpana Rajanala[1], Fabio Vilardi[1], Blanche Schwappach[1,2,‡] and Ralph H. Kehlenbach[1,‡]

ABSTRACT

Emerin is a tail-anchored protein that is found predominantly at the inner nuclear membrane (INM), where it associates with components of the nuclear lamina. Mutations in the emerin gene cause Emery–Dreifuss muscular dystrophy (EDMD), an X-linked recessive disease. Here, we report that the TRC40/GET pathway for post-translational insertion of tail-anchored proteins into membranes is involved in emerin-trafficking. Using proximity ligation assays, we show that emerin interacts with TRC40 *in situ*. Emerin expressed in bacteria or in a cell-free lysate was inserted into microsomal membranes in an ATP- and TRC40-dependent manner. Dominant-negative fragments of the TRC40-receptor proteins WRB and CAML (also known as CAMLG) inhibited membrane insertion. A rapamycin-based dimerization assay revealed correct transport of wild-type emerin to the INM, whereas TRC40-binding, membrane integration and INM-targeting of emerin mutant proteins that occur in EDMD was disturbed. Our results suggest that the mode of membrane integration contributes to correct targeting of emerin to the INM.

KEY WORDS: CAML, TRC40, WRB, Emerin, Inner nuclear membrane, Tail-anchored protein

INTRODUCTION

The nuclear envelope, which separates the nuclear and the cytoplasmic compartments, comprises three functional domains. The outer nuclear membrane (ONM) is continuous with the endoplasmic reticulum (ER) and thus equipped with a very similar set of membrane proteins and is also studded with ribosomes. In contrast, the inner nuclear membrane (INM) contains a distinct set of membrane proteins, some of which interact with the underlying nuclear lamina and/or with chromatin. Both membranes are connected at the level of the nuclear pore complex (NPC), a large multi-protein structure that mediates transport of macromolecules between the nucleus and the cytoplasm. Hence, the ONM, the INM and the small membrane patches within the NPCs can be considered as three components of a single membrane system.

A large number of proteins that are specific for, or at least enriched at, the INM have been identified, mostly by proteomic approaches (Korfali et al., 2012; Schirmer et al., 2003). One of the best-characterized INM proteins is emerin, a member of the LEM-domain family of proteins, which also contains the lamina-associated polypeptide 2 beta (LAP2β; Foisner and Gerace, 1993; Furukawa et al., 1995) and MAN1 (also known as LEMD3) (Lin et al., 2000). The LEM-domain is a helix-loop-helix fold of ∼40 amino acid residues that serves as a binding site for the chromatin-associated protein barrier to autoregulation factor (BAF, also known as BANF1). Emerin was originally identified as an X-linked gene that is mutated in patients with a certain form of Emery–Dreifuss muscular dystrophy (EDMD; Bione et al., 1994), a disease that leads to progressive skeletal muscle weakness and wasting as well as cardiomyopathies. Although a complete loss of emerin does not result in a particularly strong phenotype in knockout mice (Ozawa et al., 2006), several mutations that lead to single amino acid changes and/or frameshifts have been identified in patients affected by EDMD (see the EDMD database at http://www.dmd.nl/nmdb/home.php?select_db=EMD). Most of these mutations lead to premature termination of translation of the emerin mRNA and to loss of protein or unstable proteins (Manilal et al., 1998b; Nagano et al., 1996), although other mutations can lead to changes in the subcellular localization of emerin and aberrant functions (Ellis et al., 1998).

Emerin is a tail-anchored membrane protein of 254 residues with a single predicted transmembrane domain close to its C-terminal end and no signal peptide. Based on these topological features, the protein has been suggested to be post-translationally inserted into the cellular membrane system (Ellis et al., 1998). Such a mechanism, which is distinct from the classic pathway for signal recognition particle (SRP)-dependent insertion, was originally postulated for proteins whose C-terminal transmembrane domain cannot emerge from the ribosome before termination of translation (Kutay et al., 1993). A bioinformatics approach yielded ∼400 potential human tail-anchored proteins (Kalbfleisch et al., 2007). Most tail-anchored proteins are thought to integrate into the ER membrane, although targeting to other organelles (e.g. peroxisomes or mitochondria) is possible (Hegde and Keenan, 2011). For insertion into the ER, conserved machinery has been identified in yeast and in mammalian cells. Important players are TRC40 [transmembrane domain recognition complex protein of 40 kDa, also known as ASNA1; guided entry of tail-anchored proteins 3 (Get3) in yeast], a protein that associates with the hydrophobic stretch of amino acids at the C-terminus of tail-anchored proteins (Favaloro et al., 2008; Stefanovic and Hegde, 2007), WRB (tryptophan-rich basic protein; Get1 in yeast) (Vilardi et al., 2011) and the mammalian-specific protein CAML [Ca^{2+}-modulating cyclophilin ligand, also known as CAMLG (Yamamoto and Sakisaka, 2012)]. Together, WRB and CAML function as the TRC40 receptor at the ER membrane (Vilardi et al., 2011, 2014; Yamamoto and Sakisaka, 2012). Furthermore, chaperone-like

[1]Department of Molecular Biology, Faculty of Medicine, Georg-August-University, GZMB, Humboldtallee 23, Göttingen 37073, Germany. [2]Max-Planck Institute for Biophysical Chemistry, Göttingen 37077, Germany.
*These authors contributed equally to this work

‡Authors for correspondence (blanche.schwappach@med.uni-goettingen.de; rkehlen@gwdg.de)

Received 19 August 2015; Accepted 14 December 2015

Journal of Cell Science (2016) 129, 502-516 doi:10.1242/jcs.179333

components, such as SGTA and BAG6, capture the C-terminal transmembrane domains as they emerge from the ribosome and then deliver tail-anchored proteins to TRC40 (Leznicki et al., 2010; Mariappan et al., 2010). However, a subset of tail-anchored proteins seems to be targeted to membranes independently of the TRC40 pathway (Rabu et al., 2008) and cytochrome *b*5, for example, can be integrated into ER membranes in an unassisted manner (Colombo et al., 2009).

After membrane integration into the ER, emerin has to find its way to its final destination, the INM (Manilal et al., 1998a). Compared to nuclear import of soluble proteins, targeting of proteins to the INM is not well characterized (Burns and Wente, 2012; Ungricht and Kutay, 2015; Zuleger et al., 2012). Soullam and Worman (1995) identified specific INM-targeting signals within a nuclear region of the lamin B receptor (LBR), which comprises eight predicted transmembrane domains. Furthermore, the size of the nuclear region of the protein was suggested as a limiting factor for efficient transport to its final destination. Very recently, models that posit diffusion and retention as major determinants of INM localization of proteins have gained a lot of support (Boni et al., 2015; Ungricht et al., 2015). An energy requirement that had originally been observed for transport of proteins to the INM (Ohba et al., 2004) was attributed to ATP-dependent changes of ER structures that affect the diffusional mobility of proteins within the membrane system (Ungricht et al., 2015). In line with this interpretation, localization of emerin to the INM depends on its interaction with A-type lamins (Vaughan et al., 2001) and/or nesprins (Wheeler et al., 2007). As a result of retention at its binding site, the mobility of emerin at the INM is significantly reduced compared to that of overexpressed emerin localizing to the ER (Östlund et al., 1999). A subset of proteins, however, might also use active import pathways for transport to the INM (King et al., 2006; Kralt et al., 2015; Laba et al., 2015).

Besides the INM, emerin has been reported to localize to the peripheral ER and to the ONM, where it has been found to associate with the centrosome (Salpingidou et al., 2007), and to the plasma membrane, for example in adherens junctions of intercalated disks of cardiomyocytes (Cartegni et al., 1997). Despite this very diverse intracellular localization pattern of emerin, rather little is known about its mechanisms of membrane integration and subcellular trafficking. Early experiments with *in-vitro*-translated emerin suggested that the protein can indeed be post-translationally inserted into microsomal membranes (Ellis et al., 1998). In our study, we now provide evidence for a role of the TRC40 system in the post-translational ER membrane integration of emerin, and we analyze several emerin mutants associated with EDMD with respect to TRC40 binding, membrane integration and targeting to the INM.

RESULTS

Post-translational membrane integration of emerin by the TRC40 pathway

Emerin has been suggested to use the TRC40 pathway for membrane integration of tail-anchored proteins (Laba et al., 2014), but experimental evidence has not been available. Very recently, the crystal structure of the C-terminal transmembrane domain of the yeast tail-anchored protein Pep12 in a complex with its targeting factor Get3 has been solved (Mateja et al., 2015). The structure revealed a hydrophobic groove formed by a Get3 homodimer that shields the hydrophobic transmembrane domain of its substrate. We compared the properties of the transmembrane domains of Pep12 and emerin using a helical wheel projection (http://emboss.bioinformatics.nl/cgi-bin/emboss/pepwheel; Fig. 1A). Strikingly, six out of 20 of the characteristic amino acid residues of the transmembrane domains are identical. In addition to the typical tail-anchored protein topology, this suggests that emerin might use the mammalian homologue of Get3, TRC40, to assist in post-translational membrane integration. We therefore used a system for the purification of tail-anchored proteins in a complex with TRC40, shielding the hydrophobic transmembrane domain and protecting the tail-anchored protein from aggregation. Emerin was expressed in bacteria as a fusion protein carrying an N-terminal HZZ tag (i.e. a His tag linked to an IgG-binding ZZ-domain) and a C-terminal N-glycosylation site (an 'opsin' tag), together with maltose-binding protein (MBP)-tagged TRC40, and purified using Ni-NTA- and amylose beads (Fig. 1B). Typically, this strategy yielded ∼0.3–1.2 mg of wild-type protein per liter of bacterial culture, and the two proteins co-purified perfectly. This result demonstrates that emerin can indeed form stable complexes with TRC40.

Post-translational membrane integration of *in-vitro*-translated emerin has previously been addressed (Ellis et al., 1998). In that study, microsomal-membrane-associated emerin was sensitive to protease treatment, suggesting a type II orientation of the protein with its short C-terminal region behind the transmembrane domain facing the lumen of the microsomes. Protection of this short peptide from proteolysis, however, was not demonstrated (Ellis et al., 1998), presumably due to its small size. To unequivocally confirm post-translational membrane integration of emerin leading to a lumenal C-terminus of the protein, we took advantage of an assay where an N-glycosylation site (opsin tag) fused to the C-terminus of the protein of interest can be modified by lumenal glycosyl transferases (Pedrazzini et al., 2000). The purified MBP–TRC40 and HZZ–emerin–opsin complex was incubated with rough microsomes from dog to assess post-translational membrane integration. A shift in molecular mass indicates N-glycosylation of the reporter protein, a reaction that is specific for the ER or, in this assay, the microsomal lumen. As shown in Fig. 1C, the addition of microsomes to the reaction resulted in a significant portion of a slower migrating form of emerin as compared to a reaction lacking microsomes, indicating post-translational modification(s). Furthermore, we observed a smear of high molecular mass forms of emerin. When the sample was treated with endoglycosidase H (EndoH) after the reaction, a slow-migrating form of emerin was partially lost and the faster migrating form became more prominent, demonstrating that the protein had originally been N-glycosylated. Consequently, the opsin tag with its N-glycosylation site must have reached the microsomal lumen, confirming membrane insertion of the tail-anchored protein. Addition of lambda-phosphatase largely abolished the smear of higher molecular mass forms, in agreement with earlier observations that emerin can be phosphorylated (Ellis et al., 1998; Leach et al., 2007; Roberts et al., 2006). TRC40-dependent membrane integration of tail-anchored proteins is an active, ATP-dependent process (Favaloro et al., 2008, 2010; Stefanovic and Hegde, 2007). Accordingly, the portion of the slower migrating form of emerin was clearly reduced when ATP was omitted from the reaction (Fig. 1D,E). We also performed reactions with microsomes that had been treated with trypsin to remove potential receptor proteins from the membranes. In these assays, the fraction that shifted in molecular mass was clearly reduced, suggesting that membrane insertion of emerin occurred in a receptor-dependent manner (data not shown). Finally, the addition of fragments of the TRC40-receptor proteins WRB or CAML to the reaction almost completely prevented the shift in molecular mass (Fig. 1D,E), suggesting that

Journal of Cell Science (2016) 129, 502-516 doi:10.1242/jcs.179333

the fragments function as dominant-negative inhibitors of TRC40-mediated membrane integration, as shown previously for other tail-anchored proteins (Vilardi et al., 2011; Yamamoto and Sakisaka, 2012).

The system described above uses emerin in a pre-assembled complex with TRC40. To analyze the TRC40-dependent membrane integration of emerin in a less biased manner, we took advantage of a coupled *in vitro* transcription–translation system. As shown in Fig. 2A, emerin–opsin was synthesized *in vitro* in a plasmid-dependent manner. In the presence of rough microsomes, a shift in molecular mass was observed, which could be reversed by treating the reaction product with EndoH. Thus, the *in vitro* system

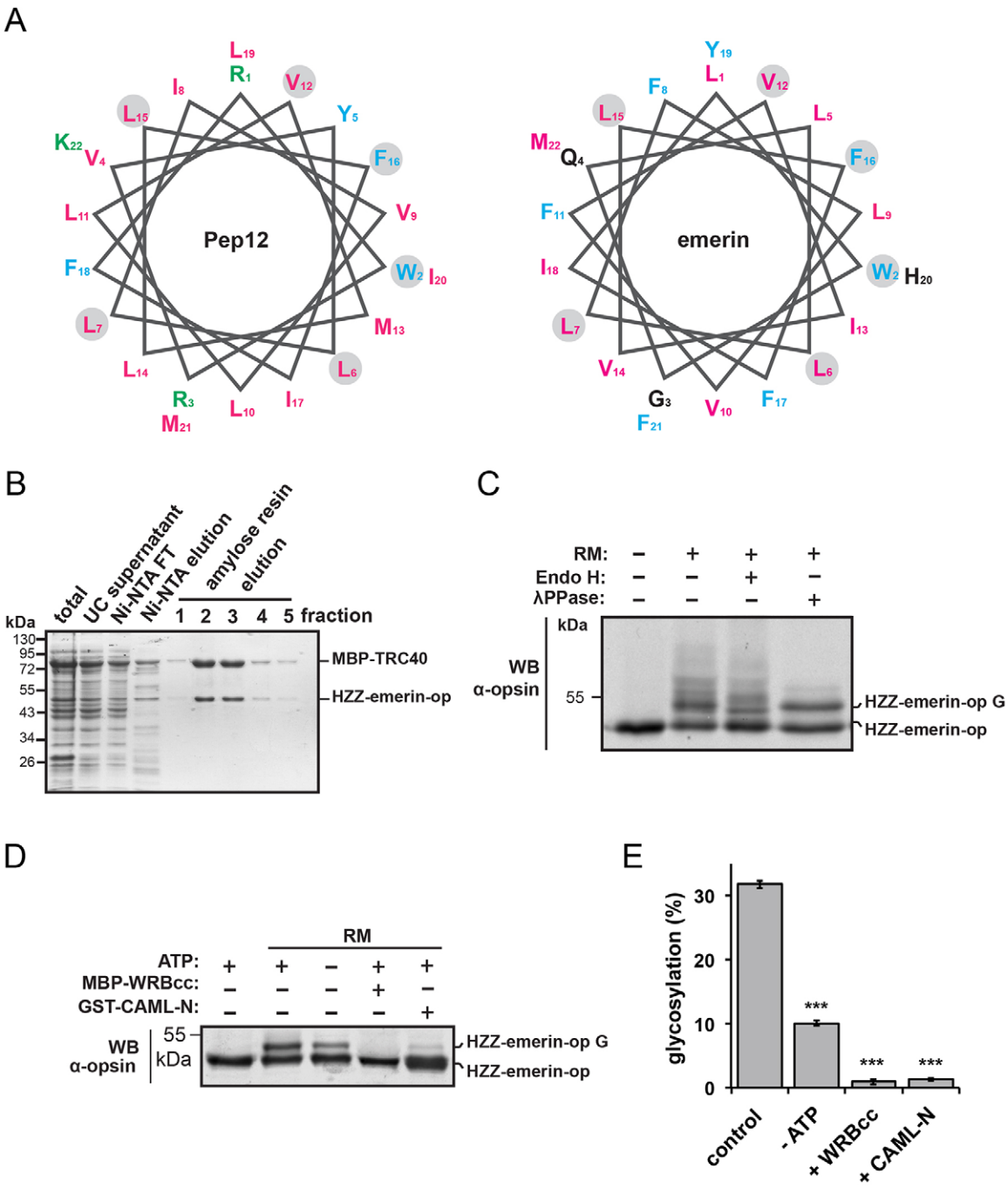

Fig. 1. The TRC40-pathway mediates the insertion of emerin into ER-enriched membranes. (A) Helical wheel projections of transmembrane domains of Pep12 and emerin. Hydrophobic residues are colored in magenta, aromatic residues in light blue and positively charged residues in green. The gray circles indicate identical residues between Pep12 and emerin. (B) Co-purification of the recombinant MBP–TRC40 and HZZ–emerin–opsin (op) complex from *E. coli* by Ni-NTA and amylose resins. UC, ultracentrifugation; FT, flow-through. (C) *In vitro* insertion of HZZ–emerin-op into rough microsomes (RM). The MBP–TRC40 and HZZ–emerin–opsin complexes were incubated with (+) or without (–) RM. Where indicated, EndoH or lambda phosphatase (λPPase) treatments were carried out after integration. WB, western blotting; G indicates the glycosylated form. (D) Effects of ATP depletion and WRBcc or CAML-N fragments (10 µM each) on membrane integration of HZZ–emerin–opsin. (E) Quantification of relative amounts of glycosylated (i.e. membrane inserted) emerin–opsin under different conditions as in D. Error bars indicate the s.d. of four independent experiments. *P<0.05; ***P<0.001 (Student's t-test).

Journal of Cell Science (2016) 129, 502-516 doi:10.1242/jcs.179333

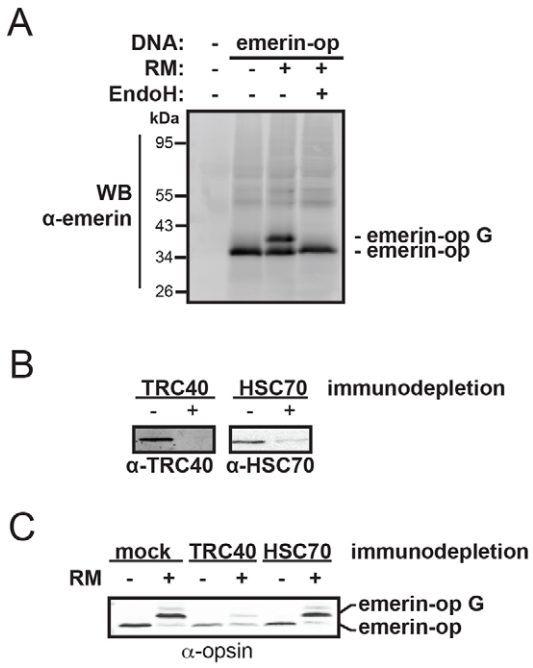

Fig. 2. *In vitro* translation and TRC40-dependent membrane insertion of emerin. (A) Opsin-tagged emerin (emerin-op) was produced *in vitro* by coupled transcription–translation in the absence (–) or presence (+) of rough microsomes (RM) and with (+) or without (–) subsequent treatment with EndoH. (B) Lysates used for coupled transcription–translation reactions were immunodepleted using antibodies against TRC40 or HSC70. (C) Depleted lysates (mock, anti-TRC40 and anti-HSC70 antibodies) were used for reactions as in A. In A–C, proteins were analyzed by SDS-PAGE, followed by immunoblotting (WB) using appropriate antibodies, as indicated. G indicates the glycosylated form.

recapitulates microsome-dependent N-glycosylation of the reporter protein and, hence, membrane integration, similar to the assay presented in Fig. 1. Next, we depleted the reticulocyte lysate that was used for *in vitro* translation using specific antibodies against TRC40 or, as a control, the chaperone HSC70 (also known as HSPA8) (Fig. 2B). Strikingly, the depletion of TRC40 from the lysate resulted in a strong reduction of N-glycosylation (i.e. membrane integration) of *in-vitro*-translated emerin compared to mock-treated or HSC70-depleted lysates (Fig. 2C). Taken together, these results show that opsin-tagged emerin can be post-translationally inserted into microsomal membranes in a TRC40-, WRB- and CAML-assisted manner.

Next, we set out to establish a membrane-integration assay for emerin in permeabilized cells. HeLa cells were treated with digitonin to preferentially permeabilize the plasma membrane and were then incubated with the purified MBP–TRC40 and HZZ–emerin–opsin complex. Similar to dog microsomes, the permeabilized cells were able to post-translationally insert emerin into ER membranes in an ATP- and temperature-dependent manner, as concluded from the observed shift in the molecular mass of the reporter protein. Again, insertion could be suppressed with WRB or CAML fragments, indicating a role for the TRC40 system (Fig. 3A). To confirm N-glycosylation as the basis for the observed shift in molecular mass, we treated the permeabilized cells with Peptide-N-glycosidase F (PNGaseF) after the first reaction. Similar to our observation with EndoH (Fig. 1C), this treatment resulted in a complete loss of the slowly migrating form of emerin with a concomitant increase in intensity of the faster migrating (i.e. deglycosylated) form (Fig. 3B).

Taken together, these results suggest post-translational membrane insertion of emerin through the TRC40–WRB–CAML system under conditions where emerin is presented to the permeabilized cells or microsomes as a preformed TRC40 complex (Figs 1 and 3) or expressed in an *in vitro* system (Fig. 2). Next, we asked whether interactions of emerin with the TRC40 system could be detected *in situ*, and we used a proximity ligation (Duolink) assay (PLA) (Söderberg et al., 2006) to address this question. This assay is based on the decoration of proteins present in a complex or in close vicinity in fixed cells with specific primary- and oligonucleotide-linked secondary antibodies. If the target proteins are in close proximity, subsequent ligation and amplification reactions lead to a fluorescent product that can easily be detected by microscopy (Söderberg et al., 2006; Fig. 4A). To demonstrate the suitability of our anti-emerin antibodies, we first set out to detect the well-established interaction of emerin with

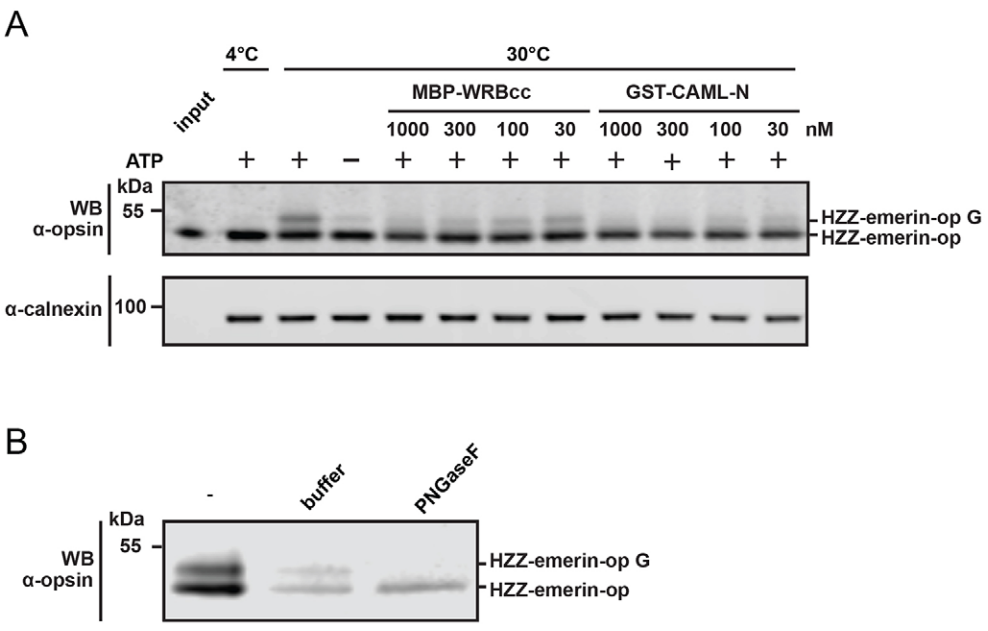

Fig. 3. Post-translational insertion of emerin into membranes of semi-permeabilized cells. (A) HeLa cells were permeabilized with digitonin and incubated with purified HZZ–emerin–opsin (op) and MBP–TRC40 at 4°C or 30°C, with or without energy (+/– ATP) and increasing amounts of MBP–WRBcc or GST–CAML-N, as indicated. (B) After a reaction as in A at 30°C in the presence of ATP, portions of the reaction were left untreated (80%, –) or further incubated with (PNGaseF) or without (buffer; 10% each) the PNGaseF. In A and B, proteins were analyzed by SDS-PAGE, followed by immunoblotting (WB) using the indicated primary antibodies. Calnexin served as a loading control. G indicates the glycosylated form of emerin.

Journal of Cell Science (2016) 129, 502-516 doi:10.1242/jcs.179333

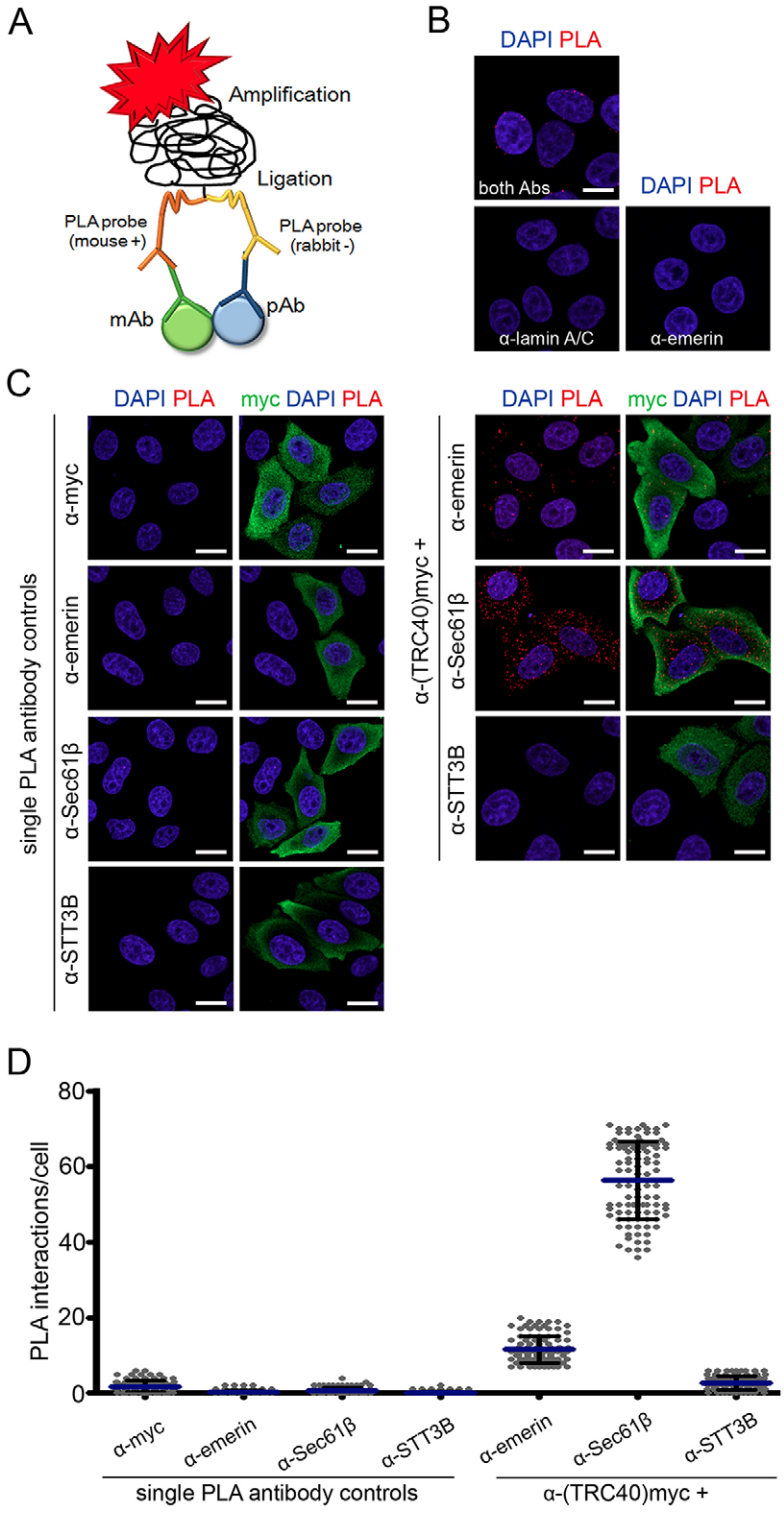

Fig. 4. *In situ* PLA detection of TRC40–emerin interactions. (A) Schematic diagram of the *in situ* PLA strategy showing primary antibodies and PLA probes binding to target proteins. Close proximity of the secondary PLA probes allows ligation followed by rolling circle amplification. (B) Intracellular localization of emerin and lamin A/C complexes using the Duolink *in situ* PLA assay in HeLa cells. PLA signals of single proteins (emerin or lamin) or protein–protein complexes (emerin–lamin) are displayed. Each red dot represents a single protein–protein interaction. Nuclei were stained with DAPI (blue) and representative images are shown. (C) HeLa cells were transfected with a plasmid coding for TRC40–Myc prior to staining with anti-Myc, -emerin, -Sec61β (positive control) or -STT3B (negative control) antibodies to detect interactions using the PLA. Cells were then stained for TRC40–Myc (green) and DAPI (blue). Left panel, negative controls, with only one primary antibody for the targeted protein–protein interaction. Right panel, dual antibody PLA. Representative confocal images are shown. Scale bars: 10 µm. (D) The dot plot represents the number of PLA dots per cell for both the single antibody controls and protein–protein interactions with mean values (blue bars) and s.d. (error bars) shown. 100 cells were scored over two independent experiments.

lamins at the INM (Vaughan et al., 2001; Fig. 4B). After fixation and permeabilization, cells were treated with antibodies against endogenous emerin and/or lamin A/C and subjected to the Duolink assay. After the reaction, red dots indicate sites where two proteins exist in proximity. When both antibodies were applied together, essentially all cells showed red fluorescent signals exclusively at the nuclear rim, indicating the interaction of emerin and lamin A/C at the INM. No signals were detected when only one of the primary antibodies was used, demonstrating the specificity of the reaction (Fig. 4B). Next, cells were transfected with Myc-tagged TRC40 and subjected to PLAs using antibodies against the Myc tag and different endogenous membrane proteins: (1) Sec61β, an established tail-anchored protein and model protein used in studying the TRC40 system (Favaloro et al., 2008; Stefanovic and Hegde, 2007); (2) STT3B, an oligosaccharyltransferase that should integrate into ER membranes with the help of the SRP; and (3) emerin. Myc–TRC40 was found in cytoplasmic regions and largely excluded from the nucleus. As shown in Fig. 4C,D, no dots were

Journal of Cell Science (2016) 129, 502-516 doi:10.1242/jcs.179333

detected in cells that had been treated with either one of the individual antibodies alone. A strong signal (~56 dots per cell) was observed with antibodies against Sec61β, our positive control, and the Myc–TRC40. The negative control, STT3B, yielded only very few dots per cell. Clearly, a specific interaction of emerin with Myc–TRC40 could be observed with an average of 12 red dots per transfected cell. For both Sec61β and emerin, the dots were mostly excluded from the nuclear region of the cells, further demonstrating the specificity of the detection.

In summary, these results show that transient interactions of emerin with TRC40 can be detected *in situ* and strongly suggest a physiological role for the TRC40 system in membrane integration of this tail-anchored protein. To further establish such a role in living cells, we established conditions for small interfering RNA (siRNA)-mediated knockdown of TRC40 and analyzed targeting of endogenous emerin to the nuclear envelope in knockdown cells and in control cells. As a control, we detected the INM protein LBR (Soullam and Worman, 1995). LBR is co-translationally inserted into the ER membrane and, hence, does not require the TRC40 pathway. Treatment of cells with specific siRNAs resulted in a clear reduction of TRC40 levels, as detected by indirect immunofluorescence (Fig. 5A,B) or western blotting (Fig. 5C). Inspection of emerin levels at the nuclear envelope revealed a clear reduction of the protein in TRC40-knockdown cells compared to control cells (Fig. 5A,B), whereas the total levels remained unchanged (Fig. 5C). LBR and STT3B, by contrast, were not affected by the siRNAs (Fig. 5A,B). These results show that targeting of emerin to the cellular membrane system is reduced in TRC40-depleted cells and they suggest that the non-targeted protein does not give rise to a strong signal in immunofluorescence microscopy.

Membrane integration of EDMD mutants of emerin

Having established the TRC40 pathway as a major route in post-translational membrane integration of emerin, we next analyzed the role of the C-terminal region of emerin in detail. Several mutations within the transmembrane domain or in its close proximity have been associated with EDMD (Ellis et al., 1998; Manilal et al., 1998b; Mora et al., 1997; Nagano et al., 1996; Nigro et al., 1995; Ognibene et al., 1999; Vohanka et al., 2001; Yates et al., 1999). We selected several emerin mutants with increasing levels of expected severity (i.e. from point mutants with single amino acid changes to mutants lacking the entire transmembrane domain; Fig. 6A). The Gln228His mutant was originally identified in a patient with X-linked mental retardation (Tarpey et al., 2009) and has not been linked to EDMD, and serves as a control for our analyses. A hydrophobicity plot of the C-terminal region of wild-type emerin and these mutants confirmed the expected changes (Fig. 6B): for the Pro183Thr, the Pro183His and the Gln228His mutant, the plot was almost identical to that of wild-type emerin. The stop codon mutation Trp226* (i.e. translation terminates after Leu225) and the frame shift mutation Leu225Arg-FS essentially abolished the transmembrane domain, whereas the Phe240His-FS mutation and the deletion ΔVal236-Phe241 resulted in shorter hydrophobic domains of the corresponding proteins. For the latter two proteins and for wild-type emerin, we also predicted ΔG-values for insertion of putative transmembrane helices into membranes (Hessa et al., 2007). The ΔG-prediction server (http://dgpred.cbr.su.se/index.php?p=home) yielded values of −4.288, −1.791 and 0.642 kcal/mol for wild-type emerin, emerin-Phe240His-FS and emerin-ΔVal236-Phe241, respectively, confirming that these mutations result in less hydrophobic transmembrane domains.

Next, we co-expressed MBP–TRC40 and wild-type (compare Fig. 1B) or mutant forms of His- and opsin-tagged emerin in bacteria (Fig. 6C). The three point mutants Pro183Thr, Pro183His and Gln228His yielded similar levels of TRC40–HZZ–emerin complexes as the wild-type protein, whereas for emerin-Trp226*, Leu225Arg-FS and Phe240His-FS, as well as the deletion ΔVal236-Phe241, substantially less HZZ–emerin–opsin was recovered during the purification, indicating reduced interaction

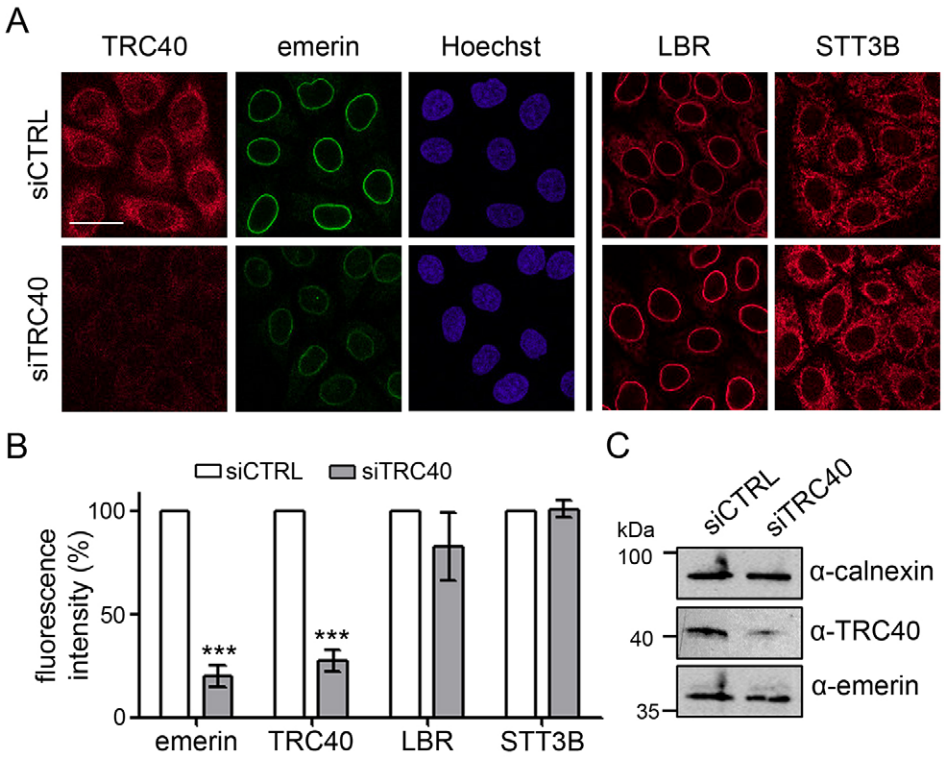

Fig. 5. Depletion of TRC40 results in reduced levels of emerin at the nuclear envelope. (A) HeLa cells were treated with a final concentration of 170 nM of specific siRNAs to reduce the levels of endogenous TRC40 (siTRC40) or control siRNAs (siCTRL) and subjected to indirect immunofluorescence detecting TRC40 and emerin or, on separate slides, LBR and STT3B, as indicated. Scale bar: 20 µm. Very similar results were obtained with siRNA concentrations as low as 50 nM. (B) Quantification of the results in A. Error bars represent the s.d. from the mean fluorescence values from 100 cells over two independent experiments. ***P<0.001 (Student's t-test). (C) Western blot of cell lysates of control cells or knockdown cells. Calnexin was used as a loading control.

Journal of Cell Science (2016) 129, 502-516 doi:10.1242/jcs.179333

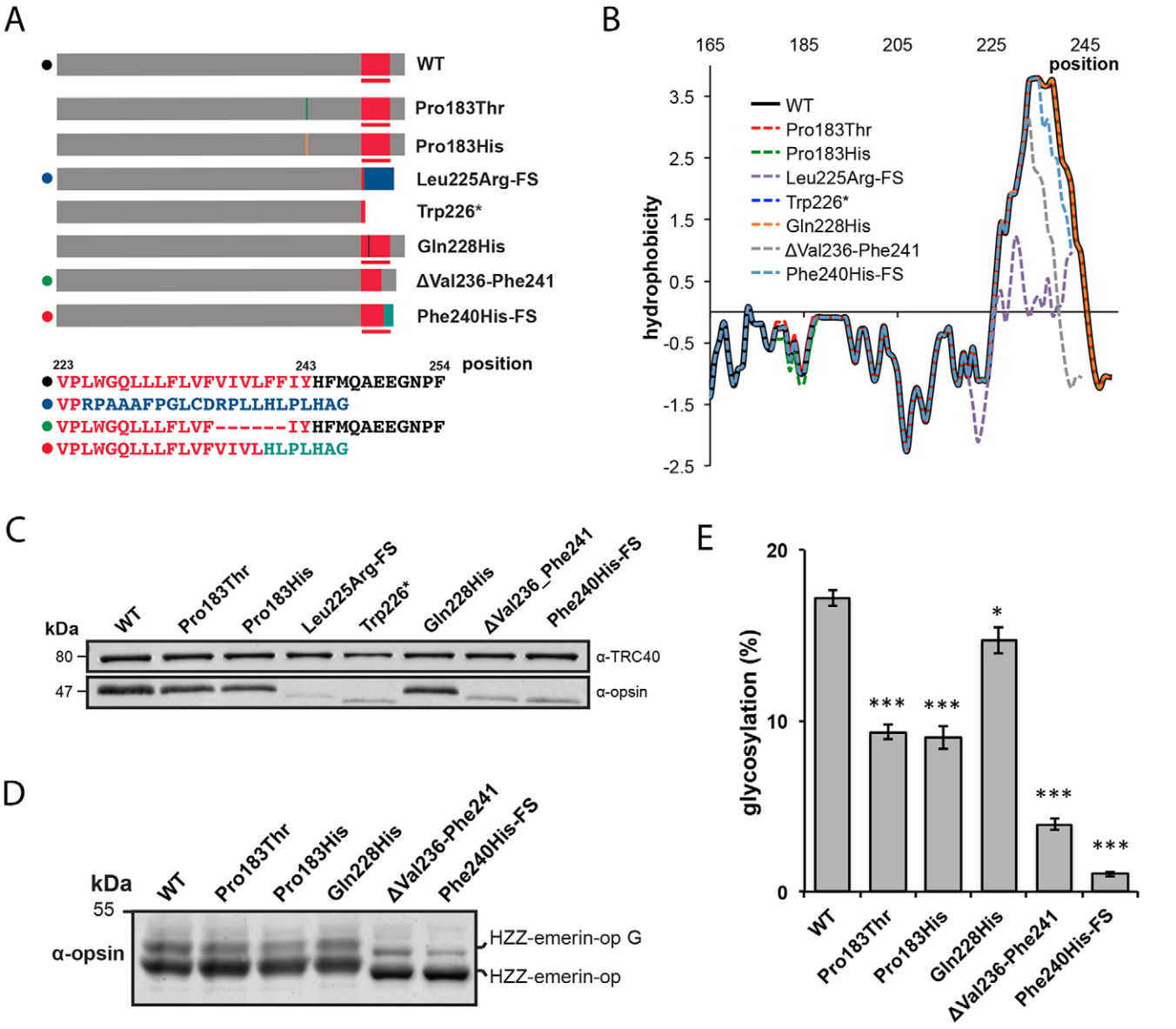

Fig. 6. Emerin disease mutants display impaired interaction with TRC40 and reduced membrane interaction. (A) Scheme of the emerin variants analyzed in this study. The transmembrane domain (TMD) is shown in red. Predicted TMDs in emerin variants are highlighted with a red line. TMDs of wild-type (WT) and Leu225Arg-FS, ΔVal236-Phe241, Phe240His-FS emerin variants are specified in detail below. (B) Kyte–Doolittle hydrophobicity plots for the C-terminal portion of the emerin mutants. (C) Co-purification of MBP–TRC40 and HZZ–emerin–opsin (op) complexes. Purified proteins were subjected to SDS-PAGE followed by western blotting detecting TRC40 and the opsin tag of the emerin variants. (D) *In vitro* insertion assay of HZZ–emerin–opsin variants into rough microsomes. Variants Trp226* and Leu225Arg-FS, which lack a transmembrane domain, were omitted from the analysis. G indicates the glycosylated form. (E) Quantification of the results in D. Relative amounts of glycosylated (i.e. membrane inserted) emerin mutants are depicted. Error bars indicate the s.d. of four independent experiments. *P<0.05; ***P<0.001 (Student's t-test).

with MBP–TRC40 (Fig. 6C). Equivalent amounts of purified emerin variants were then subjected to glycosylation assays using microsomal membranes. As shown in Fig. 6D,E, the Gln228His mutation hardly affected the degree of glycosylation (i.e. membrane integration), whereas for the Pro183Thr and Pro183His mutant, significantly less glycosylation was observed. The frame shift mutation Phe240His-FS and the deletion ΔVal236-Phe241 strongly reduced the efficiency of membrane integration of the respective proteins. These results show that TRC40-dependent membrane insertion of emerin can be affected by mutations within the transmembrane domain and, surprisingly, by single amino acid changes ~40 residues upstream of the transmembrane domain.

Targeting of emerin and emerin mutants to the INM

The most prominent localization of emerin is at the INM, although other localizations have been described. We therefore used transfection experiments and indirect immunofluorescence to compare the subcellular localization of our mutant forms of emerin with that of the wild-type protein. As expected, after fixation and Triton X-100 permeabilization of cells, HA-tagged wild-type emerin was predominantly found at the nuclear rim (Fig. 7). A similar pattern was observed for the three point mutants Pro183Thr, Pro183His and Gln228His, with some cell-to-cell variations regarding the level of extra-nuclear (i.e. presumably ER-associated) HA–emerin. The mutants Leu225Arg-FS and Trp226*

Journal of Cell Science (2016) 129, 502-516 doi:10.1242/jcs.179333

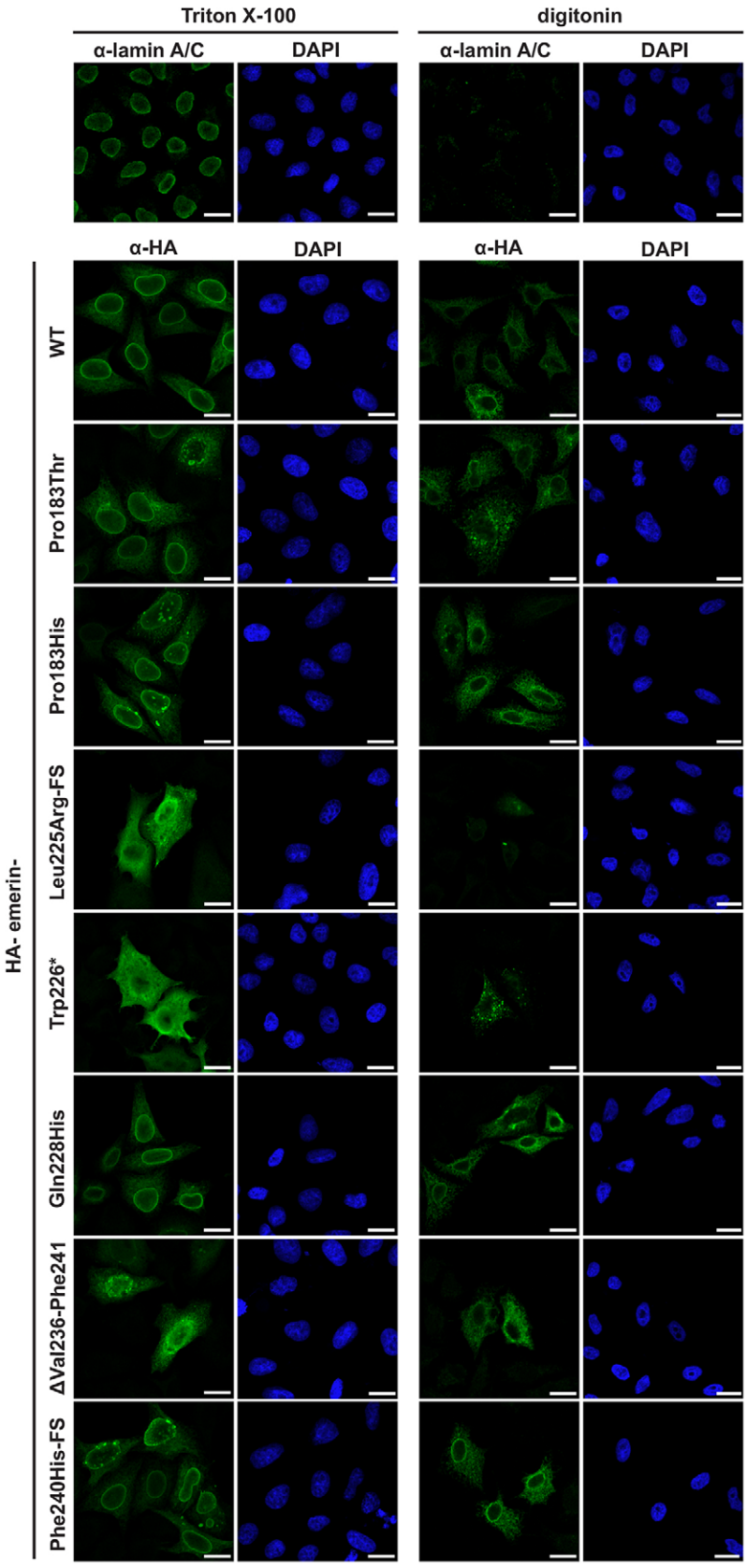

Fig. 7. Subcellular localization of emerin variants. HeLa cells were transfected with plasmids coding for HA–emerin variants, permeabilized either with Triton X-100 or digitonin and immunostained using antibodies against the HA tag. Endogenous lamin A/C immunostaining (top row) was used as a control for differential permeabilization. Scale bars: 15 µm.

as well as the deletion ΔVal236-Phe241 showed almost no localization to the nuclear rim and were found all over the cells. Interestingly, the frame shift mutant Phe240His-FS, which hardly interacted with MBP–TRC40 (Fig. 6C) and was the least efficient in the membrane integration assay (Fig. 6D,E), was found at the nuclear rim, very similar to wild-type emerin. To discriminate

Journal of Cell Science (2016) 129, 502-516 doi:10.1242/jcs.179333

between protein localization at the INM versus the ONM, we also performed immunostaining of cells subjected to differential permeabilization. Using the detergent digitonin, proteins of the INM should not be accessible to the primary antibody. Accordingly, our endogenous control protein of the INM, lamin A/C, was not detectable in digitonin-permeabilized cells, whereas a characteristic nuclear rim was observed after permeabilization with the detergent Triton X-100 (Fig. 7, top row). For HA-tagged wild-type emerin, a clear extra-nuclear signal was visible upon digitonin-treatment. Signal intensities at the nuclear rim, however, were reduced compared to Triton-X-100-treated cells, as expected. This result suggests that overexpressed HA–emerin partially reaches the INM and is partially sequestered at the ER and the ONM (as indicated by the digitonin experiment). For the Pro183 mutants and the Gln228His mutant, similar observations were made with clear, albeit weak signals, at the nuclear rim. The two emerin mutants lacking a transmembrane domain (Leu225Arg-FS and Trp226*) yielded only very weak signals in the digitonin-permeabilized cells, because the proteins are expected to be soluble and should be released from the cells upon treatment with the detergent. The deletion mutant ΔVal236-Phe241 exhibited similar signals upon Triton X-100 or digitonin treatment, without a pronounced staining at the nuclear rim. Strikingly, the emerin mutant Phe240His-FS appeared very similar in Triton-X-100- or digitonin-treated cells, with a clear nuclear rim under both conditions, suggesting that the protein localizes predominantly to the ONM. Taken together, our differential permeabilization experiments suggest that certain mutations in the emerin gene not only affect membrane integration of emerin but also its correct targeting to the INM.

To corroborate these results, we established an assay to specifically assess targeting of a reporter protein to the INM, similar to a previously published approach (Ohba et al., 2004). The system is based on induced dimerization of proteins carrying appropriate binding domains for rapamycin (Chen et al., 1995). Rapamycin binds to the 12-kDa FK506 binding protein (FKBP12) as well as a 100-amino-acid domain of mammalian target of rapamycin (mTOR), known as the FKBP-rapamycin binding domain (FRB; Fig. 8A). Thus, rapamycin should recruit a soluble nuclear reporter protein containing an FKBP12-domain (GFP_2–GST–NLS–FKBP12) to the INM if an FRB-containing protein (e.g. FRB–emerin) is present at this specific location. In our system, mCherry–FRB–emerin was expressed in cells together with GFP_2–GST–NLS–FKBP12, which showed a typical nuclear localization in the absence of rapamycin (Fig. 8B). Addition of rapamycin to the cells led to a very clear re-distribution of GFP_2–GST–NLS–FKBP12 to the nuclear periphery, resulting from drug-induced dimerization with the INM protein mCherry–FRB–emerin. As a control, we expressed WRB–FRB–HA together with the GFP reporter. At first inspection, WRB–FRB–HA showed a similar subcellular localization to mCherry–FRB–emerin, with staining in ER regions, and at the perinuclear ER and the nuclear rim. Addition of rapamycin, however, did not result in a redistribution of nuclear GFP_2–GST–NLS–FKBP12, suggesting that WRB-FRB-HA is restricted to the ER and the ONM and absent from the INM (Fig. 8B).

Next, we used this assay to analyze INM-targeting of wild-type and mutant forms of emerin (Fig. 8C). For a better comparison of targeting efficiencies (Fig. 8D), the GFP_2–GST–NLS–FKBP12 signal at the INM in rapamycin-treated cells was scored as '+++', '++', '+' and '−' (see legend for details). The two mutants lacking a transmembrane domain, mCherry–FRB–emerin-Trp226* and -Leu225Arg-FS (Fig. 6A,B), localized to the nucleus, in agreement with previous studies, where similar constructs had been used (Östlund et al., 1999; Tsuchiya et al., 1999). Consequently, rapamycin did not induce a relocalization of the GFP reporter protein to the nuclear periphery – instead, this depended on the presence of an FRB-presenting protein at the INM (Fig. 8B). The deletion mutant mCherry–FRB–emerin-ΔVal236-Phe241 was mostly found in aggregates throughout the cell and the co-expressed GFP reporter was not sequestered at the nuclear rim in the presence of rapamycin. The point mutants mCherry–FRB–emerin-Pro183Thr, -Pro183His and -Gln228His, which all localized to the nuclear rim as HA fusion proteins in a very similar fashion to wild-type emerin (see Fig. 7), also showed a similar mCherry signal to the corresponding wild-type protein (Fig. 8C). Accordingly, rapamycin induced recruitment of the GFP reporter to the INM, albeit to a lower extent compared to cells that had been co-transfected with wild-type mCherry–FRB-emerin ('++' versus '+++'). Strikingly, reduced INM targeting was even more obvious for the frame shift mutant mCherry–FRB–emerin-Phe240His-FS, which also showed a very prominent localization at the nuclear rim as an HA-tagged protein, irrespective of the permeabilization method (Fig. 7). Here, the effect of the rapamycin treatment was rather variable: in many cells (56%, 100 cells analyzed), rapamycin did not induce relocalization of GFP_2–GST–NLS–FKBP12 to the nuclear rim at all. In others, the effect was rather subtle compared to cells expressing wild-type mCherry–FRB–emerin, demonstrating that targeting to the INM was clearly impaired for this emerin mutant.

Thus, transport of emerin to or its retention at the INM depends on crucial features of the transmembrane domain or the luminal C-terminus and, potentially, on additional single amino acid residues in its close proximity. The assay shows that all disease mutants investigated reduce the fidelity with which emerin reaches its final destination, the INM. Localization at the nuclear rim, as observed for emerin mutants in previous studies (Fairley et al., 1999; Lee et al., 2001) is clearly not equivalent to correct targeting to the INM.

DISCUSSION

In this study, we analyzed membrane insertion and targeting of emerin to the INM and several clinically relevant emerin mutants linked to EDMD. The TRC40 pathway is the most prominent route for post-translational membrane integration of tail-anchored proteins, although other pathways that are promoted by HSC70 or HSP40 (Rabu et al., 2008) or the SRP (Abell et al., 2004, 2007) have been described. Furthermore, membrane insertion can occur through unassisted pathways that do not depend on additional soluble and/or membrane-bound factors (Brambillasca et al., 2006; Colombo et al., 2009). Upon co-expression in bacteria, emerin and TRC40 formed a stable complex (Fig. 1B), suggesting that emerin can also be captured by TRC40 as soon as it emerges from the translating ribosome in eukaryotic cells. Accordingly, depletion of TRC40 from reticulocyte lysates resulted in a clearly reduced membrane insertion of emerin (Fig. 2C). Given that the interaction of tail-anchored proteins with components of the TRC40 machinery is rather transient, it has been difficult to detect by classical co-immunoprecipitation approaches. However, PLAs corroborated our findings, showing that endogenous emerin interacts with overexpressed TRC40, albeit with lower signal numbers than endogenous Sec61β. In this assay, the number of dots that are scored as single interaction sites depends on (among other factors) the abundance of the individual proteins and on the quality of the specific antibodies. Hence, a quantitative comparison of the

Journal of Cell Science

Journal of Cell Science (2016) 129, 502-516 doi:10.1242/jcs.179333

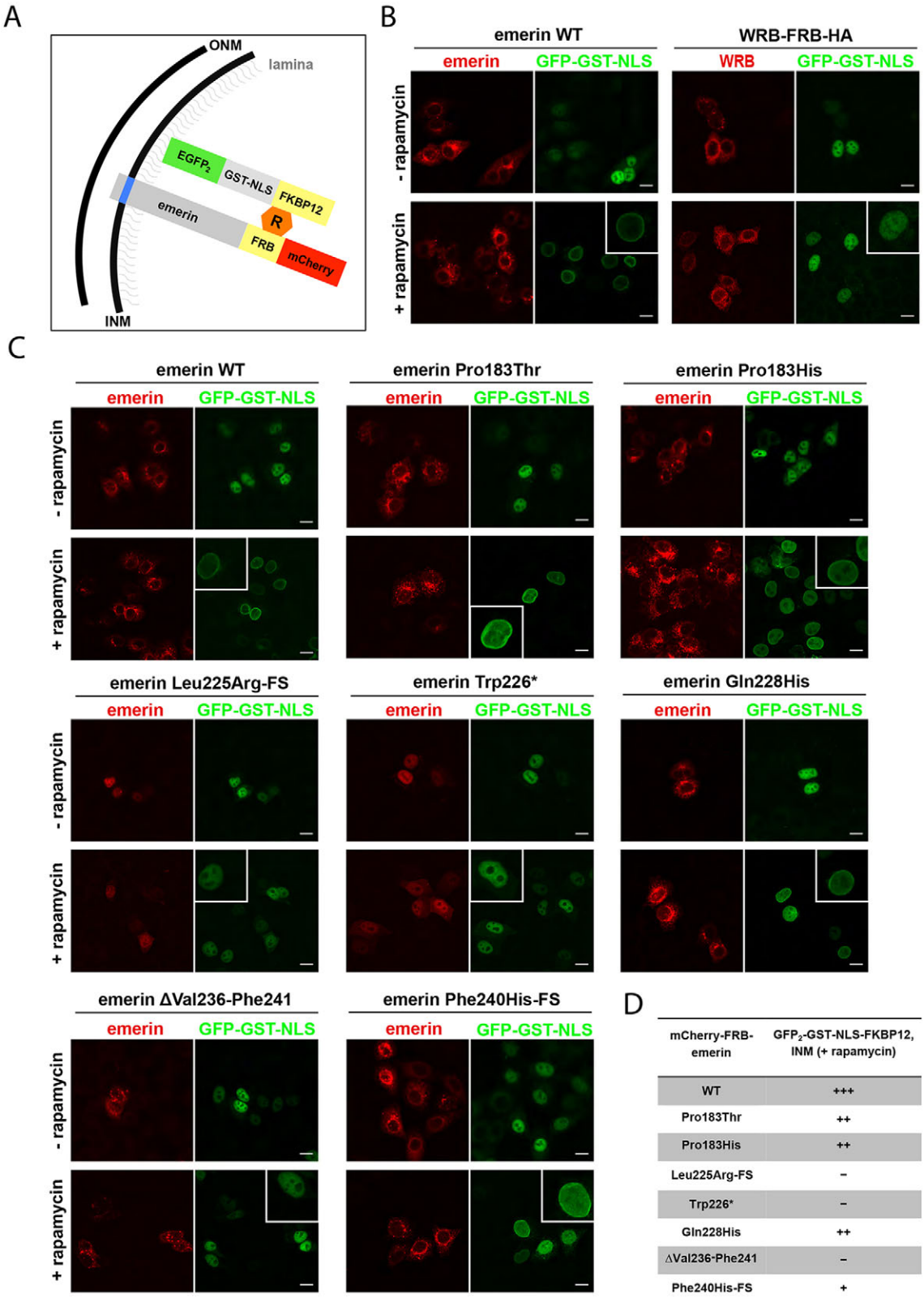

Fig. 8. Mutations in the emerin gene affect targeting to the INM. (A) Rapamycin assay. Upon rapamycin (R) treatment, the soluble nuclear $EGFP_2$–GST–NLS–FKBP12 reporter is recruited to mCherry–FRB–emerin at the INM. (B,C) HeLa cells were co-transfected with constructs coding for $EGFP_2$–GST–NLS–FKBP12 (GFP-GST-NLS) and WRB–FRB–HA (WRB; B) or variants of mCherry–FRB–emerin (emerin; B,C), permeabilized with digitonin and treated with (+) or without (–) rapamycin. WT, wild-type. After fixation, cells were analyzed by confocal microscopy, either directly (emerin) or after immunostaining (WRB-FRB-HA). Scale bars, 15 µm. Typical cells at higher magnification (+ rapamycin) are shown in the inserts. Note that under our assay conditions (10 min on ice), the GFP reporter protein does not exit from the nucleus. (D) Semi-quantitative analysis of the rapamycin-effect on $EGFP_2$–GST–NLS-FKBP12. +++, clear rim in essentially all cells; ++, visible rim in most cells but residual nuclear signal; +, visible rim in some cells, signal mostly nuclear; and –, no nuclear rim). Between 20 (Trp226*) and 100 cells (WT, Phe240His-FS) from separate experiments were scored.

Journal of Cell Science (2016) 129, 502-516 doi:10.1242/jcs.179333

interaction of the two tail-anchored proteins with TRC40 is not possible. Nevertheless, for Sec61β as well as for emerin, the signals were specific and almost exclusively detected in the cytoplasmic region of the cells, consistent with interactions occurring at or close to ER membranes. PLAs have been used previously for the detection of TRC40 binding to tail-anchored proteins (Hradsky et al., 2011), but, to our knowledge, only upon overexpression of both interacting partners. Here, we used antibodies against endogenous emerin to monitor binding to lamin A/C as well as Myc-tagged TRC40. Hence, this assay should be applicable for the analysis of interactions between other tail-anchored proteins and TRC40 or other components of the TRC40 machinery.

Our integration assays using microsomes (Figs 1, 2 and 6) or permeabilized cells (Fig. 3) clearly confirmed the possibility of post-translational membrane insertion of opsin-tagged emerin in a TRC40-, WRB- and CAML-assisted manner. The permeabilized cell system should be useful for future approaches, e.g. for analysis of membrane insertion upon knockdown of certain components of the TRC40 machinery. Our *in vivo* experiments with TRC40-depleted cells (Fig. 5) further strengthen these findings. Of course, we cannot rule out the possibility that in cells lacking TRC40, membrane insertion of emerin is supported by alternative post-translational mechanisms. In summary, we provide experimental evidence for emerin as the first tail-anchored protein of the INM that uses the TRC40 pathway for membrane insertion.

Several studies have analyzed the role of specific properties of individual transmembrane domains as well as of neighboring regions on post-translational membrane insertion of tail-anchored proteins (Beilharz et al., 2003; Borgese et al., 2001). As expected, emerin mutants with a complete loss of (Trp226*) or with drastic changes within the transmembrane domain (Leu225Arg-FS, ΔVal236-Phe241, Phe240His-FS) showed strongly reduced binding to TRC40 (Fig. 6C) and impaired membrane insertion in the microsome assay (Fig. 6C,D). Accordingly, HA-tagged emerin-Trp226*, -Leu225Arg-FS and -ΔVal236-Phe241 did not show a prominent localization at the nuclear envelope in transfection experiments (Fig. 7). Surprisingly, however, HA–emerin-Phe240His-FS was found at the nuclear rim, very similar to the wild-type protein, although it showed strongly reduced insertion efficiency into ER-derived microsomes (Fig. 6D,E). Perhaps this mutant with its shortened transmembrane domain and a less negative ΔG-value for membrane insertion (−1.791 compared to −4.288 kcal/mol for wild-type emerin) is able to insert into the cellular membrane system in an unassisted manner or with the help of certain chaperones that are present in intact cells but not in the microsome assay. Similar results have been described for protein tyrosine phosphatase 1B, whose transmembrane domain is less hydrophobic than that of emerin (Brambillasca et al., 2006). Similarly, the emerin mutants Pro183Thr and Pro183His showed slightly reduced binding to TRC40 and significantly reduced membrane insertion (Fig. 6C,D), yet the localization of HA-tagged proteins appeared normal (Fig. 7). The transmembrane domains of these mutants are identical to that of wild-type emerin, suggesting that residues upstream of the hydrophobic stretch can affect the interaction with TRC40. For the corresponding GFP-tagged emerin mutants, reduced levels of fluorescence at the nuclear rim have been described previously (Fairley et al., 1999). Correct targeting to the INM, as opposed to the ONM was, however, not analyzed in that study. Our immunofluorescence results after differential permeabilization (Fig. 7) and the results of the rapamycin assay (Fig. 8C,D) now suggest that the emerin-Pro183 mutants and, in particular, the Phe240His-FS mutant have impaired targeting to the INM, although, at the level of light microscopy, their localization pattern at the nuclear envelope was similar to that of the wild-type protein.

The exact route of emerin (or other proteins of the INM) from the ER via the ONM and the NPC to the INM is not known. With respect to molecular mechanisms, two very recent publications (Boni et al., 2015; Ungricht et al., 2015) have shown that passive diffusion followed by subsequent retention at the target site are major determinants of INM localization. Nevertheless, energy-dependent changes in ER morphology have been suggested to affect the transport rates of proteins to the INM (Ungricht et al., 2015) and are also expected to affect proteins that are post-translationally inserted into the ER membrane. Selected proteins, by contrast, seem to require more active, transport-factor-dependent mechanisms (Laba et al., 2015). Transmembrane proteins that are co-translationally inserted into the ER membrane must passage through the NPCs in a membrane-bound form, possibly through dedicated, peripheral channels (Maimon et al., 2012). For tail-anchored proteins, it is principally possible that they are imported into the nucleus as soluble complexes with TRC40, followed by direct insertion into the INM from within the nuclear interior. In light of the low nuclear levels of TRC40 (Fig. 4C), the rather few PLA signals revealing emerin–TRC40 interactions inside the nucleus (Fig. 4C) and the apparent absence of the receptor protein WRB from the INM (Fig. 8B), this route seems rather unlikely. Instead, emerin is probably inserted into the ER system as a default membrane for tail-anchored proteins. From the ER, it is expected to traffic to the INM via the ONM and the NPC. Emerin as well as several other proteins of the INM contain putative nuclear localization signals (NLSs) and emerin fragments lacking the transmembrane domain were found to accumulate in the nucleus as a result of the NLS activity (Östlund et al., 1999; Tsuchiya et al., 1999). The significance of these NLSs and also of their cognate receptor proteins (e.g. importin α and β) for trafficking of membrane-bound proteins across the NPC, however, remains unclear.

In intact cells, the different mutant emerin variants that we tested reached the INM with efficiencies that cannot entirely be predicted by the efficiency of membrane insertion into microsomes. Thus, our results might suggest that membrane insertion of emerin through the TRC40 pathway and trafficking of the protein to the INM are sequential processes with distinct requirements. However, the major determinants for proper localization of emerin to the INM have been localized to regions outside of the transmembrane domain (Östlund et al., 1999; Tsuchiya et al., 1999). Our observations thus raise the interesting possibility that integration through the TRC40 pathway affects the correct targeting of emerin to its final destination, beyond initial membrane insertion. Perhaps the emerin mutant Phe240His-FS reaches the ONM by an alternative pathway that is not compatible with probing the INM and its constituent proteins. In summary, the molecular pathogenesis of EDMD as caused by the different mutations is likely to be complex. Damaging effects might result from reduced levels of functional emerin in the INM or from toxicity caused by mislocalized emerin variants. Given that interaction with nuclear proteins is key to emerin functions (Demmerle et al., 2012), mislocalization to the ONM or the ER is expected to contribute to the pathologic phenotypes of certain emerin mutants. Furthermore, mislocalization of tail-anchored proteins to the outer membrane of mitochondria has been recognized as a potential mechanism of toxicity in yeast and mammalian cells (Chen et al., 2014; Okreglak and Walter, 2014; Schuldiner et al., 2008). It will be necessary to consider these different possible causes of disease when further elucidating the

Journal of Cell Science (2016) 129, 502-516 doi:10.1242/jcs.179333

targeting of wild-type emerin and its mutant variants in the pertinent differentiated cells, like skeletal muscle cells or cardiomyocytes.

MATERIALS AND METHODS

Plasmids and constructs

All constructs were obtained using standard methods and verified by sequencing. The vector for coexpression of MBP–TRC40 and an HZZ-tagged tail-anchored protein was as described previously (Favaloro et al., 2010). Briefly, the coding sequence of human emerin was amplified by PCR using emerin–GFP (obtained from Eric Schirmer, Edinburgh, UK) as a template and forward (5′-TTTGGTACCACCATGGACAACTACGC-AGATCTT-3′) and reverse (5′-CAAGCTTTATCAGCCCGTCTTGTTG-GAGAAAGGCACGTAGAAGTTTGGGCCGAAGGGGTTGCCTTCTT-CAG-3′) primers, the latter also coding for an opsin tag. The PCR-product was cloned into a modified pET-vector (pET328) through KpnI and HindIII, generating a fusion construct with an N-terminal HZZ tag (pET328-HZZ-Emerin-opsin). The modified emerin-sequence was then cut with AvrII and NheI and cloned into a pQE80-vector that also codes for MBP–TRC40, generating pQE80-MBP-TRC40/HZZ-emerin-opsin. For pEF-HA-emerin, the emerin coding sequence was amplified from emerin–GFP and cloned into pEF-HA (Gasteier et al., 2003) through SpeI and NcoI. To generate pGEM3Z-Emerin-opsin, a KpnI–HindIII fragment from pET328-HZZ-Emerin-opsin was cloned into pGEM3Z.

Emerin mutants Pro183His, Pro183Thr, Leu225Arg-FS, Trp226*, Gln228His, ΔVal236-Phe241 and Phe240His-FS were generated in pQE80-MBP-TRC40/HZZ-emerin-opsin and in pEF-HA-emerin by Quikchange site-directed mutagenesis (Braman et al., 1996) or SPRINP methods (Edelheit et al., 2009), using appropriate oligonucleotides (list available upon request).

The FKBP12 sequence for the plasmid coding for $EGFP_2$–GST–NLS–FKBP12 was obtained by PCR amplification from pcDNA3-FKBP12 (Belshaw et al., 1996) and inserted into a pEGFP-C1-derivative coding for $EGFP_2$–GST–NLS (kindly provided by Detlef Doenecke, Göttingen, Germany) through BamHI and XbaI.

Human FRB (the minimal FKBP12-rapamycin-binding domain from FRAP, 2025–2114 fragment; Chen et al., 1995) was PCR amplified from CD4-FRAP-pcDNA3 and cloned into pmCherry-C1 (Clontech) through BglII and XhoI, generating pmCherry-FRB. The emerin sequence was then introduced through XhoI and BamH1, generating pmCherry-FRB-emerin.

Emerin mutants as above were amplified from pEF-HA-emerin mutant vectors and cloned into pmCherry-FRB through XhoI and BamHI. The point mutation pmCherry-FRB-emerin Gln228His was generated by Quikchange mutagenesis in pmCherry-FRB-emerin-WT. To obtain pcDNA-WRB-FRB-HA, the sequences for human WRB and FRB were PCR-amplified from pRK5-WRB-HA (Vilardi et al., 2011) and pmCherry-FRB and cloned through NheI-HindIII or HindIII-BamHI, respectively, into a pcDNA3.1(+) derivative containing an HA tag.

Expression and purification of proteins

Recombinant MBP-TRC40/HZZ-emerin variant complexes were obtained as described previously (Favaloro et al., 2010) with some modifications. *E. coli* BL21AI cells were transformed with pQE80-MBP-TRC40/HZZ-emerin-opsin variants. Expression of MBP–TRC40 was induced at an optical density at 600 nm (OD_{600}) of 0.5 with 50 µM IPTG for 1 h at 30°C, followed by induction of HZZ–emerin expression with 0.25% arabinose for 4 h. Cells were harvested and lysed by sonification in cold LS buffer (50 mM Hepes, 150 mM potassium acetate, 5 mM $Mg(OAc)_2$, 10% glycerol, 1 mM PMSF, 1 mM DTT, pH 7.0) supplemented with 20 mM imidazole and 10 µg/ml DNase I. The lysate was cleared at 100,000 ***g*** for 30 min and incubated with a Ni-NTA resin. After 1 h, the resin was sequentially washed with LS buffer supplemented with 5 mM ATP, HS buffer (50 mM Hepes, 500 mM KOAc, 5 mM $Mg(OAc)_2$, 10% glycerol, 1 mM PMSF, 1 mM DTT, pH 7.0) and LS buffer. All washing buffers were supplemented with 20 mM imidazole. The proteins were eluted with LS buffer containing 300 mM imidazole and incubated with an amylose resin for 1 h. The resin was washed with LS buffer supplemented with 5 mM ATP, with HS buffer and again with LS buffer, and the recombinant complex was eluted with LS buffer containing 20 mM maltose.

Expression of the terminal cytosolic domain of CAML (GST–CAML-N) (Yamamoto and Sakisaka, 2012) and of the coiled-coil domain of WRB (MBP–WRBcc) (Vilardi et al., 2011) was as described previously.

Cell culture, transfections and immunofluorescence microscopy

HeLa P4 cells (Charneau et al., 1994), were obtained from the NIH AIDS Reagent Program and were grown in DMEM (Gibco) supplemented with 10% (v/v) FCS (Gibco), 100 U/ml penicillin, 100 µg/ml streptomycin, and 2 mM L-glutamine (Gibco) under 5% CO_2 at 37°C. They were tested for contamination by mycoplasma on a regular basis. For immunofluorescence, cells were grown on poly-L-lysine-coated coverslips and transfected with the calcium phosphate method (Chen and Okayama, 1987) unless specified otherwise. For siRNA-mediated knockdown, cells were transfected with Lipofectamine (Invitrogen) for 48 h according to manufacturer's instructions using siRNAs against TRC40 (s1675, Ambion) or a non-targeting control siRNA (AM4635, Ambion).

Cells were fixed with 3.7% (v/v) formaldehyde in PBS and permeabilized with 0.5% Triton X-100 in PBS for 5 min on ice, except for the differential permeabilization experiments. Samples were blocked with either 2% BSA or 10% FCS in PBS for 30 min and incubated with primary antibodies diluted in blocking buffer for 1.5 h at room temperature. Incubation with secondary antibodies was performed for 1 h in blocking buffer at room temperature. In siRNA experiments, cells were fixed in 100% methanol at −20°C for 5 min.

Cells were mounted with Mowiol-DAPI and analyzed using an Axiovert 200 M fluorescence microscope with a 63× Plan-Neofluar 1.3 NA water-corrected objective and appropriate filter settings. Images were taken using an LSM 510-META confocal laser scanning microscope (Zeiss) and processed using ImageJ and Adobe Photoshop 6.0.

For quantification of the knockdown effects on the fluorescent signal, a small circle was drawn at the nuclear envelope or in the cytoplasm and fluorescence intensities were determined after background subtraction. Averages were calculated for each treatment group and plotted relative to the highest value (control siRNA), which was set to 100%.

Antibodies and western blotting

For immunodepletions, rat monoclonal anti-HSC70 (1:1000, Stressgen) and rabbit anti-TRC40 (Favaloro et al., 2010) antibodies were used. For indirect immunofluorescence, mouse anti-HA antibodies (1:1000, Convance or Sigma), mouse-anti-TRC40 (1:200, Sigma), rabbit anti-emerin (1:300, Proteintech), rabbit-anti-LBR (1:300, Proteintech), rabbit-anti-STT3B (kind gift from Stephen High, Manchester) and anti-lamin A/C (1:200, Abcam) were used as primary antibodies and donkey-anti-mouse-IgG conjugated to Alexa Fluor 488 or 594 (1:1000; Molecular Probes) as secondary antibodies. Mouse anti-opsin (Adamus et al., 1991), rabbit anti-calnexin (1:1000, Enzo), rabbit-anti-TRC40 (1:1000, Proteintech) and rabbit-anti emerin (1:1000, Santa Cruz Biotechnology) antibodies were used for immunoblotting. For the PLA, mouse anti-myc (1:1000; Santa Cruz Biotechnology), rabbit anti-emerin (1:2000, Proteintech), rabbit anti-Sec61β (kind gift from Bernhard Dobberstein, Heidelberg), rabbit anti-STT3B or mouse anti-lamin A/C (1:1000, Abcam) antibodies were used. Western blotting was performed according to standard methods using the Odyssey system (Licor) for secondary antibody detection. For siRNA experiments, chemiluminescence (Millipore) was used. Statistical significance of the data was analyzed by a two-tailed Student's *t*-test. $P<0.05$ was considered as biologically significant.

Microsome integration assay

Membrane integration of emerin variants was evaluated as previously described (Favaloro et al., 2010; Vilardi et al., 2011). Briefly, two equivalents of rough microsomes (Walter and Blobel, 1983) were incubated for 1 h at 30°C with 200 ng of HZZ–emerin–opsin and MBP–TRC40 complexes in a final volume of 20 µl in the absence or presence of 1 mM ATP.

Where indicated, MBP–WRB coiled-coil domain (MBP-WRBcc) or the GST–CAML-N terminal cytosolic domain (GST-CAML-N) were added to a final concentration of 10 µM. In some experiments, glycosylation or phosphorylation of opsin-tagged emerin was confirmed by treatment of the samples with either 1000 units of EndoH (New England Biolabs), or 400 units of lambda phosphatase (New England Biolabs), in a final volume of

40 µl, according to the instructions of the manufacturer. The efficiency of membrane integration was monitored by SDS-PAGE, followed by western blotting and signal detection using the Odyssey system (Licor). In order to avoid the interference of phosphorylated emerin in the quantification of glycosylation, lambda phosphatase treatment was carried out after the insertion. Signals were quantified using Image Studio Lite (Licor) and expressed as the percentage of N-glycosylated emerin compared with total emerin. Statistical significance of the data was analyzed as above.

Membrane integration in permeabilized cells

HeLa P4 cells grown on plastic dishes were trypsinized and washed with culture medium and PBS. 4×10^6 cells were resuspended in 400 µl transport buffer [TPB; 20 mM HEPES, 110 mM KOAc, 2 mM $Mg(OAc)_2$, 1 mM EGTA, pH 7.3, 2 mM DTT, 0.1 mM PMSF and 1 µg/ml each of leupeptin, pepstatin and aprotinin] and permeabilized with a final concentration of 0.01% digitonin. Cells were washed three times with TPB and resuspended in TPB at 10,000 cells/µl. In a reaction volume of 100 µl, 200,000 cells were incubated with 200 ng of the MBP–TRC40 and HZZ–emerin-WT complex and 1 mM lithium-ATP (Roche) for 1 h at 30°C, followed by centrifugation at 16,000 ***g*** for 20 min. After one washing step with TPB, the cells were dissolved in SDS sample buffer and subjected to SDS-PAGE and immunoblotting. For deglycosylation, cells were treated with 500 units PNGaseF (NEB) in a 20 µl reaction after membrane integration.

Proximity ligation assay

HeLa cells were transfected with a plasmid coding for TRC40-myc using Lipofectamine 2000 (Invitrogen). At 48 h post transfection, cells were fixed and permeabilized as described above. Cells were then subjected to the proximity ligation assay (PLA) using the Duolink red kit (O-link Bioscience) in a humidity chamber according to the manufacturer's instructions. Briefly, cells were blocked, incubated with appropriate primary antibodies and thereafter incubated with PLA probes, which are secondary antibodies (anti-mouse-IgG and anti-rabbit-IgG) conjugated to unique oligonucleotides. Samples were then treated with a ligation solution (allowing oligonucleotide pairs in close proximity to form a closed circle) followed by an amplification solution containing polymerase and fluorescently labeled oligonucleotides, allowing rolling-circle amplification and detection of discrete fluorescent dots. After the PLA protocol, cells were counterstained with anti-Myc monoclonal antibody (Santa Cruz Biotechnology) and Alexa-Fluor-488-conjugated (Molecular Probes) secondary antibody to visualize TRC40–Myc transfected cells. Cells were mounted using Duolink mounting medium with DAPI (O-link Bioscience) and analyzed by confocal laser scanning microscopy with a 63× water objective. 100 cells, over two independent experiments, were imaged for analysis and each red dot was scored as a single interaction site by eye or using the Duolink Image Tool software.

Differential permeabilization assay

HeLa cells were transfected with plasmids coding for HA-tagged emerin variants and permeabilized either with 0.007% digitonin in TPB for 5 min on ice prior to fixation with 3.7% formaldehyde in PBS or first fixed and then permeabilized with 0.3% Triton X-100 and 0.05% SDS in PBS for 10 min at room temperature. Cells were then subjected to immunofluorescence microscopy.

Rapamycin assay

HeLa cells were grown on coverslips and transfected with plasmids coding for $EGFP_2$–GST–NLS–FKBP12 and an FRB-containing protein of interest. After 24 h, they were permeabilized with 0.007% digitonin in TPB containing protease inhibitors for 5 min on ice, washed in TPB and treated with 200 nM rapamycin (Sigma) in TPB for 10 min on ice. Cells were washed again with PBS, fixed with 3.7% formaldehyde in PBS and subjected to immunofluorescence microscopy.

Coupled *in vitro* transcription and translation

Reactions were performed in the TnT Quick Coupled Transcription/Translation System (Promega). Briefly, 200 ng of plasmid DNA (pGEM3Z-Emerin-opsin) was used and the reaction was carried out for 90 min at 30°C. 25% of the reaction was separated by SDS-PAGE for immunodetection. Immunodepletion of TRC40 or HSC70 was performed as described previously (Johnson et al., 2012).

Acknowledgements

We are grateful to Stephen High (Manchester) and Bernhard Dobberstein (Heidelberg) for reagents and Stephen High for very helpful discussions. We also wish to thank Lena Musiol for critical reading of the manuscript.

Competing interests

The authors declare no competing or financial interests.

Author contributions

J.P., J.R.M., C.J., F.V., B.S and R.H.K. designed research; J.P., J.R.M., C.J., K.R., F.V. and R.H.K. performed research; J.P., J.R.M., C.J., K.R., F.V., B.S and R.H.K. analyzed data; J.P., J.R.M., R.H.K. and B.S. wrote the paper.

Funding

This study was supported by grants of the Deutsche Forschungsgemeinschaft [grant numbers KE 660/12-1 to R.H.K. and SFB1002, TP B01, to B.S.]; and by the People Progamme (Marie Curie Actions) of the European Union's Seventh Framework Programme (FP7/2007-2013/) under the Research Executive Agency [grant number 607072 to B.S. and J.R.M.].

References

Abell, B. M., Pool, M. R., Schlenker, O., Sinning, I. and High, S. (2004). Signal recognition particle mediates post-translational targeting in eukaryotes. *EMBO J.* **23**, 2755-2764.

Abell, B. M., Rabu, C., Leznicki, P., Young, J. C. and High, S. (2007). Post-translational integration of tail-anchored proteins is facilitated by defined molecular chaperones. *J. Cell Sci.* **120**, 1743-1751.

Adamus, G., Zam, Z. S., Arendt, A., Palczewski, K., McDowell, J. H. and Hargrave, P. A. (1991). Anti-rhodopsin monoclonal antibodies of defined specificity: characterization and application. *Vision Res.* **31**, 17-31.

Beilharz, T., Egan, B., Silver, P. A., Hofmann, K. and Lithgow, T. (2003). Bipartite signals mediate subcellular targeting of tail-anchored membrane proteins in Saccharomyces cerevisiae. *J. Biol. Chem.* **278**, 8219-8223.

Belshaw, P. J., Ho, S. N., Crabtree, G. R. and Schreiber, S. L. (1996). Controlling protein association and subcellular localization with a synthetic ligand that induces heterodimerization of proteins. *Proc. Natl. Acad. Sci. USA* **93**, 4604-4607.

Bione, S., Maestrini, E., Rivella, S., Mancini, M., Regis, S., Romeo, G. and Toniolo, D. (1994). Identification of a novel X-linked gene responsible for Emery-Dreifuss muscular dystrophy. *Nat. Genet.* **8**, 323-327.

Boni, A., Politi, A. Z., Strnad, P., Xiang, W., Hossain, M. J. and Ellenberg, J. (2015). Live imaging and modeling of inner nuclear membrane targeting reveals its molecular requirements in mammalian cells. *J. Cell Biol.* **209**, 705-720.

Borgese, N., Gazzoni, I., Barberi, M., Colombo, S. and Pedrazzini, E. (2001). Targeting of a tail-anchored protein to endoplasmic reticulum and mitochondrial outer membrane by independent but competing pathways. *Mol. Biol. Cell* **12**, 2482-2496.

Braman, J., Papworth, C. and Greener, A. (1996). Site-directed mutagenesis using double-stranded plasmid DNA templates. *Methods Mol. Biol.* **57**, 31-44.

Brambillasca, S., Yabal, M., Makarow, M. and Borgese, N. (2006). Unassisted translocation of large polypeptide domains across phospholipid bilayers. *J. Cell Biol.* **175**, 767-777.

Burns, L. T. and Wente, S. R. (2012). Trafficking to uncharted territory of the nuclear envelope. *Curr. Opin. Cell Biol.* **24**, 341-349.

Cartegni, L., di Barletta, M. R., Barresi, R., Squarzoni, S., Sabatelli, P., Maraldi, N., Mora, M., Di Blasi, C., Cornelio, F., Merlini, L. et al. (1997). Heart-specific localization of emerin: new insights into Emery-Dreifuss muscular dystrophy. *Hum. Mol. Genet.* **6**, 2257-2264.

Charneau, P., Mirambeau, G., Roux, P., Paulous, S., Buc, H. and Clavel, F. (1994). HIV-1 reverse transcription. A termination step at the center of the genome. *J. Mol. Biol.* **241**, 651-662.

Chen, C. and Okayama, H. (1987). High-efficiency transformation of mammalian cells by plasmid DNA. *Mol. Cell. Biol.* **7**, 2745-2752.

Chen, J., Zheng, X. F., Brown, E. J. and Schreiber, S. L. (1995). Identification of an 11-kDa FKBP12-rapamycin-binding domain within the 289-kDa FKBP12-rapamycin-associated protein and characterization of a critical serine residue. *Proc. Natl. Acad. Sci. USA* **92**, 4947-4951.

Chen, Y.-C., Umanah, G. K. E., Dephoure, N., Andrabi, S. A., Gygi, S. P., Dawson, T. M., Dawson, V. L. and Rutter, J. (2014). Msp1/ATAD1 maintains mitochondrial function by facilitating the degradation of mislocalized tail-anchored proteins. *EMBO J.* **33**, 1548-1564.

Colombo, S. F., Longhi, R. and Borgese, N. (2009). The role of cytosolic proteins in the insertion of tail-anchored proteins into phospholipid bilayers. *J. Cell Sci.* **122**, 2383-2392.
Demmerle, J., Koch, A. J. and Holaska, J. M. (2012). The nuclear envelope protein emerin binds directly to histone deacetylase 3 (HDAC3) and activates HDAC3 activity. *J. Biol. Chem.* **287**, 22080-22088.
Edelheit, O., Hanukoglu, A. and Hanukoglu, I. (2009). Simple and efficient site-directed mutagenesis using two single-primer reactions in parallel to generate mutants for protein structure-function studies. *BMC Biotechnol.* **9**, 61.
Ellis, J. A., Craxton, M., Yates, J. R. and Kendrick-Jones, J. (1998). Aberrant intracellular targeting and cell cycle-dependent phosphorylation of emerin contribute to the Emery-Dreifuss muscular dystrophy phenotype. *J. Cell Sci.* **111**, 781-792.
Fairley, E. A., Kendrick-Jones, J. and Ellis, J. A. (1999). The Emery-Dreifuss muscular dystrophy phenotype arises from aberrant targeting and binding of emerin at the inner nuclear membrane. *J. Cell Sci.* **112**, 2571-2582.
Favaloro, V., Spasic, M., Schwappach, B. and Dobberstein, B. (2008). Distinct targeting pathways for the membrane insertion of tail-anchored (TA) proteins. *J. Cell Sci.* **121**, 1832-1840.
Favaloro, V., Vilardi, F., Schlecht, R., Mayer, M. P. and Dobberstein, B. (2010). Asna1/TRC40-mediated membrane insertion of tail-anchored proteins. *J. Cell Sci.* **123**, 1522-1530.
Foisner, R. and Gerace, L. (1993). Integral membrane proteins of the nuclear envelope interact with lamins and chromosomes, and binding is modulated by mitotic phosphorylation. *Cell* **73**, 1267-1279.
Furukawa, K., Pante, N., Aebi, U. and Gerace, L. (1995). Cloning of a cDNA for lamina-associated polypeptide 2 (LAP2) and identification of regions that specify targeting to the nuclear envelope. *EMBO J.* **14**, 1626-1636.
Gasteier, J. E., Madrid, R., Krautkrämer, E., Schröder, S., Muranyi, W., Benichou, S. and Fackler, O. T. (2003). Activation of the Rac-binding partner FHOD1 induces actin stress fibers via a ROCK-dependent mechanism. *J. Biol. Chem.* **278**, 38902-38912.
Hegde, R. S. and Keenan, R. J. (2011). Tail-anchored membrane protein insertion into the endoplasmic reticulum. *Nat. Rev. Mol. Cell Biol.* **12**, 787-798.
Hessa, T., Meindl-Beinker, N. M., Bernsel, A., Kim, H., Sato, Y., Lerch-Bader, M., Nilsson, I., White, S. H. and von Heijne, G. (2007). Molecular code for transmembrane-helix recognition by the Sec61 translocon. *Nature* **450**, 1026-1030.
Hradsky, J., Raghuram, V., Reddy, P. P., Navarro, G., Hupe, M., Casado, V., McCormick, P. J., Sharma, Y., Kreutz, M. R. and Mikhaylova, M. (2011). Post-translational membrane insertion of tail-anchored transmembrane EF-hand Ca2+ sensor calneurons requires the TRC40/Asna1 protein chaperone. *J. Biol. Chem.* **286**, 36762-36776.
Johnson, N., Vilardi, F., Lang, S., Leznicki, P., Zimmermann, R. and High, S. (2012). TRC40 can deliver short secretory proteins to the Sec61 translocon. *J. Cell Sci.* **125**, 3612-3620.
Kalbfleisch, T., Cambon, A. and Wattenberg, B. W. (2007). A bioinformatics approach to identifying tail-anchored proteins in the human genome. *Traffic* **8**, 1687-1694.
King, M. C., Patrick Lusk, C. and Blobel, G. (2006). Karyopherin-mediated import of integral inner nuclear membrane proteins. *Nature* **442**, 1003-1007.
Korfali, N., Wilkie, G. S., Swanson, S. K., Srsen, V., de las Heras, J., Batrakou, D. G., Malik, P., Zuleger, N., Kerr, A. R. W., Florens, L. et al. (2012). The nuclear envelope proteome differs notably between tissues. *Nucleus* **3**, 552-564.
Kralt, A., Jagalur, N. B., van den Boom, V., Lokareddy, R. K., Steen, A., Cingolani, G., Fornerod, M. and Veenhoff, L. M. (2015). Conservation of inner nuclear membrane targeting sequences in mammalian Pom121 and yeast Heh2 membrane proteins. *Mol. Biol. Cell* **26**, 3301-3312.
Kutay, U., Hartmann, E. and Rapoport, T. A. (1993). A class of membrane proteins with a C-terminal anchor. *Trends Cell Biol.* **3**, 72-75.
Laba, J. K., Steen, A. and Veenhoff, L. M. (2014). Traffic to the inner membrane of the nuclear envelope. *Curr. Opin. Cell Biol.* **28**, 36-45.
Laba, J. K., Steen, A., Popken, P., Chernova, A., Poolman, B. and Veenhoff, L. M. (2015). Active nuclear import of membrane proteins revisited. *Cells* **4**, 653-673.
Leach, N., Bjerke, S. L., Christensen, D. K., Bouchard, J. M., Mou, F., Park, R., Baines, J., Haraguchi, T. and Roller, R. J. (2007). Emerin is hyperphosphorylated and redistributed in herpes simplex virus type 1-infected cells in a manner dependent on both UL34 and US3. *J. Virol.* **81**, 10792-10803.
Lee, K. K., Haraguchi, T., Lee, R. S., Koujin, T., Hiraoka, Y. and Wilson, K. L. (2001). Distinct functional domains in emerin bind lamin A and DNA-bridging protein BAF. *J. Cell Sci.* **114**, 4567-4573.
Leznicki, P., Clancy, A., Schwappach, B. and High, S. (2010). Bat3 promotes the membrane integration of tail-anchored proteins. *J. Cell Sci.* **123**, 2170-2178.
Lin, F., Blake, D. L., Callebaut, I., Skerjanc, I. S., Holmer, L., McBurney, M. W., Paulin-Levasseur, M. and Worman, H. J. (2000). MAN1, an inner nuclear membrane protein that shares the LEM domain with lamina-associated polypeptide 2 and emerin. *J. Biol. Chem.* **275**, 4840-4847.
Maimon, T., Elad, N., Dahan, I. and Medalia, O. (2012). The human nuclear pore complex as revealed by cryo-electron tomography. *Structure* **20**, 998-1006.
Manilal, S., Man, N. t. and Morris, G. E. (1998a). Colocalization of emerin and lamins in interphase nuclei and changes during mitosis. *Biochem. Biophys. Res. Commun.* **249**, 643-647.
Manilal, S., Recan, D., Sewry, C. A., Hoeltzenbein, M., Llense, S., Leturcq, F., Deburgrave, N., Barbot, J.-C., Man, N., Muntoni, F. et al. (1998b). Mutations in Emery-Dreifuss muscular dystrophy and their effects on emerin protein expression. *Hum. Mol. Genet.* **7**, 855-864.
Mariappan, M., Li, X., Stefanovic, S., Sharma, A., Mateja, A., Keenan, R. J. and Hegde, R. S. (2010). A ribosome-associating factor chaperones tail-anchored membrane proteins. *Nature* **466**, 1120-1124.
Mateja, A., Paduch, M., Chang, H.-Y., Szydlowska, A., Kossiakoff, A. A., Hegde, R. S. and Keenan, R. J. (2015). Protein targeting. Structure of the Get3 targeting factor in complex with its membrane protein cargo. *Science* **347**, 1152-1155.
Mora, M., Cartegni, L., Di Blasi, C., Barresi, R., Bione, S., di Barletta, M. R., Morandi, L., Merlini, L., Nigro, V., Politano, L. et al. (1997). X-linked Emery-Dreifuss muscular dystrophy can be diagnosed from skin biopsy or blood sample. *Ann. Neurol.* **42**, 249-253.
Nagano, A., Koga, R., Ogawa, M., Kurano, Y., Kawada, J., Okada, R., Hayashi, Y. K., Tsukahara, T. and Arahata, K. (1996). Emerin deficiency at the nuclear membrane in patients with Emery-Dreifuss muscular dystrophy. *Nat. Genet.* **12**, 254-259.
Nigro, V., Bruni, P., Ciccodicola, A., Polltano, L., Nigro, G., Piluso, G., Cappa, V., Covone, A. E., Romeo, G. and D'Urso, M. (1995). SSCP detection of novel mutations in patients with Emery-Dreifuss muscular dystrophy: definition of a small C-terminal region required for emerin function. *Hum. Mol. Genet.* **4**, 2003-2004.
Ognibene, A., Sabatelli, P., Petrini, S., Squarzoni, S., Riccio, M., Santi, S., Villanova, M., Palmeri, S., Merlini, L. and Maraldi, N. M. (1999). Nuclear changes in a case of X-linked Emery-Dreifuss muscular dystrophy. *Muscle Nerve* **22**, 864-869.
Ohba, T., Schirmer, E. C., Nishimoto, T. and Gerace, L. (2004). Energy- and temperature-dependent transport of integral proteins to the inner nuclear membrane via the nuclear pore. *J. Cell Biol.* **167**, 1051-1062.
Okreglak, V. and Walter, P. (2014). The conserved AAA-ATPase Msp1 confers organelle specificity to tail-anchored proteins. *Proc. Natl. Acad. Sci. USA* **111**, 8019-8024.
Östlund, C., Ellenberg, J., Hallberg, E., Lippincott-Schwartz, J. and Worman, H. J. (1999). Intracellular trafficking of emerin, the Emery-Dreifuss muscular dystrophy protein. *J. Cell Sci.* **112**, 1709-1719.
Ozawa, R., Hayashi, Y. K., Ogawa, M., Kurokawa, R., Matsumoto, H., Noguchi, S., Nonaka, I. and Nishino, I. (2006). Emerin-lacking mice show minimal motor and cardiac dysfunctions with nuclear-associated vacuoles. *Am. J. Pathol.* **168**, 907-917.
Pedrazzini, E., Villa, A., Longhi, R., Bulbarelli, A. and Borgese, N. (2000). Mechanism of residence of cytochrome b(5), a tail-anchored protein, in the endoplasmic reticulum. *J. Cell Biol.* **148**, 899-914.
Rabu, C., Wipf, P., Brodsky, J. L. and High, S. (2008). A precursor-specific role for Hsp40/Hsc70 during tail-anchored protein integration at the endoplasmic reticulum. *J. Biol. Chem.* **283**, 27504-27513.
Roberts, R. C., Sutherland-Smith, A. J., Wheeler, M. A., Norregaard Jensen, O., Emerson, L. J., Spiliotis, II, Tate, C. G., Kendrick-Jones, J. and Ellis, J. A. (2006). The Emery-Dreifuss muscular dystrophy associated-protein emerin is phosphorylated on serine 49 by protein kinase A. *FEBS J.* **273**, 4562-4575.
Salpingidou, G., Smertenko, A., Hausmanowa-Petrucewicz, I., Hussey, P. J. and Hutchison, C. J. (2007). A novel role for the nuclear membrane protein emerin in association of the centrosome to the outer nuclear membrane. *J. Cell Biol.* **178**, 897-904.
Schirmer, E. C., Florens, L., Guan, T., Yates, J. R., III and Gerace, L. (2003). Nuclear membrane proteins with potential disease links found by subtractive proteomics. *Science* **301**, 1380-1382.
Schuldiner, M., Metz, J., Schmid, V., Denic, V., Rakwalska, M., Schmitt, H. D., Schwappach, B. and Weissman, J. S. (2008). The GET complex mediates insertion of tail-anchored proteins into the ER membrane. *Cell* **134**, 634-645.
Söderberg, O., Gullberg, M., Jarvius, M., Ridderstråle, K., Leuchowius, K.-J., Jarvius, J., Wester, K., Hydbring, P., Bahram, F., Larsson, L.-G. et al. (2006). Direct observation of individual endogenous protein complexes in situ by proximity ligation. *Nat. Methods* **3**, 995-1000.
Soullam, B. and Worman, H. J. (1995). Signals and structural features involved in integral membrane protein targeting to the inner nuclear membrane. *J. Cell Biol.* **130**, 15-27.
Stefanovic, S. and Hegde, R. S. (2007). Identification of a targeting factor for posttranslational membrane protein insertion into the ER. *Cell* **128**, 1147-1159.
Tarpey, P. S., Smith, R., Pleasance, E., Whibley, A., Edkins, S., Hardy, C., O'Meara, S., Latimer, C., Dicks, E., Menzies, A. et al. (2009). A systematic, large-scale resequencing screen of X-chromosome coding exons in mental retardation. *Nat. Genet.* **41**, 535-543.
Tsuchiya, Y., Hase, A., Ogawa, M., Yorifuji, H. and Arahata, K. (1999). Distinct regions specify the nuclear membrane targeting of emerin, the responsible protein for Emery-Dreifuss muscular dystrophy. *Eur. J. Biochem.* **259**, 859-865.

Ungricht, R. and Kutay, U. (2015). Establishment of NE asymmetry—targeting of membrane proteins to the inner nuclear membrane. *Curr. Opin. Cell Biol.* **34**, 135-141.
Ungricht, R., Klann, M., Horvath, P. and Kutay, U. (2015). Diffusion and retention are major determinants of protein targeting to the inner nuclear membrane. *J. Cell Biol.* **209**, 687-704.
Vaughan, A., Alvarez-Reyes, M., Bridger, J. M., Broers, J. L., Ramaekers, F. C., Wehnert, M., Morris, G. E., Whitfield, W. G. F. and Hutchison, C. J. (2001). Both emerin and lamin C depend on lamin A for localization at the nuclear envelope. *J. Cell Sci.* **114**, 2577-2590.
Vilardi, F., Lorenz, H. and Dobberstein, B. (2011). WRB is the receptor for TRC40/Asna1-mediated insertion of tail-anchored proteins into the ER membrane. *J. Cell Sci.* **124**, 1301-1307.
Vilardi, F., Stephan, M., Clancy, A., Janshoff, A. and Schwappach, B. (2014). WRB and CAML are necessary and sufficient to mediate tail-anchored protein targeting to the ER membrane. *PLoS ONE* **9**, e85033.
Vohanka, S., Vytopil, M., Bednarik, J., Lukas, Z., Kadanka, Z., Schildberger, J., Ricotti, R., Bione, S. and Toniolo, D. (2001). A mutation in the X-linked Emery–Dreifuss muscular dystrophy gene in a patient affected with conduction cardiomyopathy. *Neuromuscul. Disord.* **11**, 411-413.
Walter, P. and Blobel, G. (1983). Preparation of microsomal membranes for cotranslational protein translocation. *Methods Enzymol.* **96**, 84-93.
Wheeler, M. A., Davies, J. D., Zhang, Q., Emerson, L. J., Hunt, J., Shanahan, C. M. and Ellis, J. A. (2007). Distinct functional domains in nesprin-1alpha and nesprin-2beta bind directly to emerin and both interactions are disrupted in X-linked Emery–Dreifuss muscular dystrophy. *Exp. Cell Res.* **313**, 2845-2857.
Yamamoto, Y. and Sakisaka, T. (2012). Molecular machinery for insertion of tail-anchored membrane proteins into the endoplasmic reticulum membrane in mammalian cells. *Mol. Cell* **48**, 387-397.
Yates, J. R. W., Bagshaw, J., Aksmanovic, V. M. A., Coomber, E., McMahon, R., Whittaker, J. L., Morrison, P. J., Kendrick-Jones, J. and Ellis, J. A. (1999). Genotype-phenotype analysis in X-linked Emery–Dreifuss muscular dystrophy and identification of a missense mutation associated with a milder phenotype. *Neuromuscul. Disord.* **9**, 159-165.
Zuleger, N., Kerr, A. R. W. and Schirmer, E. C. (2012). Many mechanisms, one entrance: membrane protein translocation into the nucleus. *Cell. Mol. Life Sci.* **69**, 2205-2216.